Leishmania infantum exploits the anti-ferroptosis effects of Nrf2 to escape cell death in macrophages

Clément Blot, Mathilde Lavernhe, Geanncarlo Lugo-Villarino, Kimberley Coulson, Marie Salon, Margot Tertrais, Rémi Planès, Karin Santoni, Hélène Authier, Godefroy Jacquemin, et al.

Cell Reports

Article

Leishmania infantum exploits the anti-ferroptosis effects of Nrf2 to escape cell death in macrophages

Graphical abstract

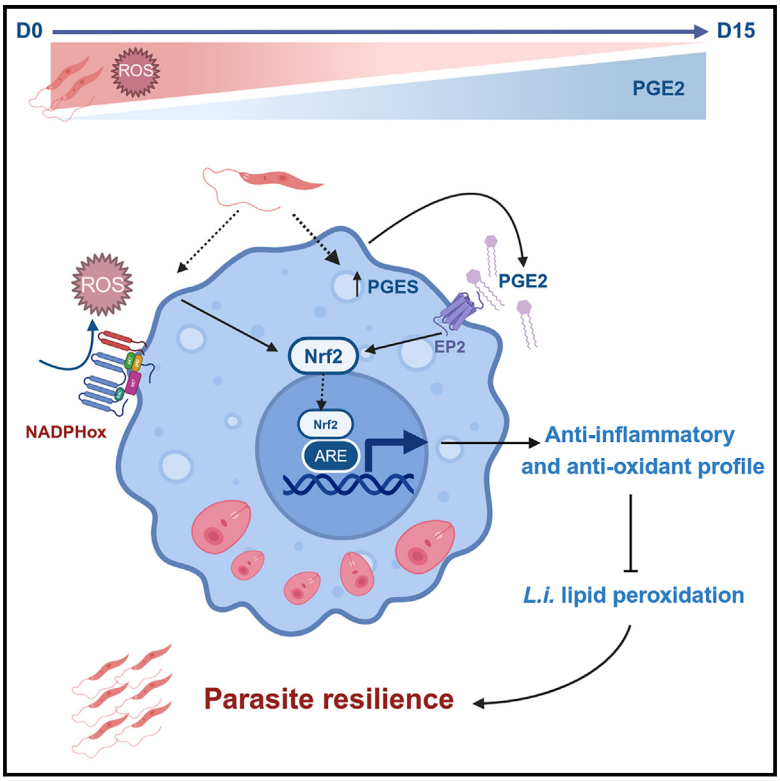

Highlights

- ROS and the PGE2/EP2 axis mediate Nrf2 activation in MΦs to promote *L.i.* growth
- Nrf2 promotes *L.i.* infection via an anti-oxidant and anti-inflammatory profile of MΦs
- Nrf2 in MΦs protects *L.i.* from lipid peroxidation, preventing its death by ferroptosis

Authors

Clément Blot, Mathilde Lavernhe, Geanncarlo Lugo-Villarino, ..., Etienne Meunier, Lise Lefèvre, Agnès Coste

Correspondence

lise.lefevre@univ-tlse3.fr (L.L.), agnes.coste@univ-tlse3.fr (A.C.)

In brief

Blot et al. demonstrate that Nrf2 is a critical transcription factor that protects *Leishmania infantum* from lipid peroxidation and death by a ferroptosis-like process through the induction of an anti-oxidant and anti-inflammatory profile of macrophages. Hence, pharmacological inhibition of Nrf2 constitutes a promising target for the treatment of visceral leishmaniasis.

Blot et al., 2024, Cell Reports *43*, 114720
September 24, 2024
https://doi.org/10.1016/j.celrep.2024.114720

CellPress

Cell Reports

CellPress
OPEN ACCESS

Article

Leishmania infantum exploits the anti-ferroptosis effects of Nrf2 to escape cell death in macrophages

Clément Blot,[1] Mathilde Lavernhe,[1] Geanncarlo Lugo-Villarino,[2] Kimberley Coulson,[1] Marie Salon,[1] Margot Tertrais,[1] Rémi Planès,[2] Karin Santoni,[2] Hélène Authier,[1] Godefroy Jacquemin,[1] Mouna Rahabi,[1] Mélissa Parny,[1] Isabelle Raymond Letron,[1] Etienne Meunier,[2,3] Lise Lefèvre,[1,3,4,*] and Agnès Coste[1,3,*]

[1]RESTORE UMR 1301-INSERM 5070 CNRS EFS UPS, Toulouse, France

[2]Institute of Pharmacology and Structural Biology (IPBS), UMR5089 CNRS UPS, Toulouse, France

[3]These authors contributed equally

[4]Lead contact

*Correspondence: lise.lefevre@univ-tlse3.fr (L.L.), agnes.coste@univ-tlse3.fr (A.C.)

https://doi.org/10.1016/j.celrep.2024.114720

SUMMARY

Macrophages are major host cells for the protozoan *Leishmania* parasite. Depending on their activation state, they either contribute to the detection and elimination of *Leishmania* spp. or promote parasite resilience. Here, we report that the activation of the transcription factor nuclear factor erythroid 2-related factor 2 (Nrf2) in macrophages plays a pivotal role in the progression of *Leishmania infantum* infection by controlling inflammation and redox balance of macrophages. We also highlight the involvement of the NOX2/reactive oxygen species (ROS) axis in early Nrf2 activation and, subsequently, prostaglandin E2 (PGE2)/EP2r signaling in the sustenance of Nrf2 activation upon infection. Moreover, we establish a ferroptosis-like process within macrophages as a cell death program of *L. infantum* and the protective effect of Nrf2 in macrophages against *L. infantum* death. Altogether, these results identify Nrf2 as a critical factor for the susceptibility of *L. infantum* infection, highlighting Nrf2 as a promising pharmacological target for the development of therapeutic approaches for the treatment of visceral leishmaniasis.

INTRODUCTION

Leishmania species are intracellular protozoan parasites that cause multiple diseases, ranging from non-lethal cutaneous leishmaniasis to severe visceral disease, if left untreated.[1] *Leishmania infantum* (*L.i*.) is one of the major parasite species associated with visceral leishmaniasis.[2] Macrophages are the major myeloid-derived immune cells that contribute to the detection and elimination of *Leishmania* spp. However, they are also the primary replication sites for these parasites by providing them an environment suitable to their life cycle.[3] Macrophages can control *L.i.* infection through the generation of reactive oxygen species (ROS),[4] underscoring the critical role of redox balance in determining the disease's clinical outcome. The transcriptional master regulator of cellular responses against oxidative stress, known as nuclear factor erythroid 2-related factor 2 (Nrf2), is among the key factors that regulate the redox balance.[5] Indeed, Nrf2 controls the expression of multiple anti-oxidant and phase II enzyme genes.[6] Furthermore, Nrf2 activation limits inflammation by decreasing the transcription of pro-inflammatory cytokines through nuclear factor κB (NF-κB)-based dependent and independent pathways.[7,8]

A wide variety of intracellular pathogens, such as viruses, bacteria, and protozoan parasites, enhance Nrf2 activation, thus leading to immune tolerance.[9–11] It is well established that cutaneous and visceral forms of leishmaniasis upregulate the Nrf2 pathway in macrophages in response to parasite-induced ROS production.[12] Thus, in the early stages of parasite infection, ROS-generated activation of Nrf2 constitutes a strategy developed by the parasite to subvert exposure to oxidants and survive in macrophages.[13]

The regulation of Nrf2 expression by *Leishmania* strains increases SOD1 and HO-1 anti-oxidant genes, thereby promoting parasite persistence. Indeed, the establishment of a visceral infection by *L. donovani* is dependent on the induction of HO-1 by Nrf2.[12,14] This leads to a decrease in the cellular heme content, thus inhibiting the maturation of nicotinamide adenine dinucleotide phosphate (NADPH) oxidase subunits, which then suppresses ROS production and participates in parasite survival in macrophages.[15] Although some reports linked macrophage ROS production to *Leishmania* elimination, the cell death program involved in the ROS-mediated killing of *Leishmania*[4] has not been explored so far. Interestingly, glutathione peroxidase 4 (GPX4), which is an identified transcriptional target of Nrf2, is crucial in the regulation of iron-dependent non-apoptotic modes of cell death, termed ferroptosis.[16] Indeed, GPX4 prevents the accumulation of toxic lipid ROS and thereby blocks the onset of ferroptosis.[17,18] Interestingly, the lethal phenotype of *Trypanosoma brucei*

that lacks the tryparedoxin peroxidases, distant relatives of GPX4 in higher eukaryotes,[19] strongly suggests that the ferroptosis cell death program occurs in *Leishmania* spp. parasites.[20]

While the activation of Nrf2 by *Leishmania* strains is well documented, the precise molecular mechanisms involved in this activation are not yet fully understood.[12] However, a previous study proposed that *Leishmania donovani* facilitates an immunosuppressive environment in macrophages through prostaglandin E2 (PGE2)/EP2 receptor signaling.[21] Moreover, PGE2 secretion by macrophages in response to microbial infections, such as that of the Kaposi's sarcoma-associated herpes virus (KSHV), is also reported. In this context, PGE2 production upon viral infection leads to the activation of Nrf2, resulting in a permissive microenvironment for KSHV.[22]

Based on the different studies that underscore the crucial role of Nrf2 in macrophage-mediated control of *L.i.* infection, we hypothesized that the oxidative burst and PGE2 secretion by *Leishmania*-infected macrophages could activate Nrf2, ultimately promoting the progression of infection by protecting the parasite against ferroptotic cell death.

The objective of our study was to investigate the role of the Nrf2 pathway *L.i.* infection. Specifically, we aimed to elucidate the molecular mechanism responsible for activating the Nrf2 signaling pathway in macrophages in response to *L.i.* Pharmacological inhibition, or genetic deletion, of Nrf2 allowed us to define this transcription factor as a major player in the progression of *L.i.* infection through its impact in the control of inflammation and redox balance of macrophages. Our findings shed light on the crucial signaling pathways involved in the activation and maintenance of Nrf2 activation during *L.i.* infection; that is, while the NOX2/ROS axis is crucial during the early stages of infection, the PGE2/EP2 axis plays a pivotal role in the maintenance of Nrf2 activation at the later stages. Moreover, we also demonstrated that Nrf2 activity in macrophages protects *L.i.* from lipid peroxidation, preventing the death of parasites by a ferroptosis-like process. Finally, these pathways were also pertinent during infection of primary human macrophages, inferring that Nrf2 may be a potential target for the treatment of visceral leishmaniasis.

RESULTS

L.i. triggers ROS and PGE2 production leading to Nrf2 activation

We previously showed that ROS production affects *Leishmania* survival.[4] Based on these results, we investigated the mRNA level of NADPH oxidase subunits and iNOS in macrophages from C57BL/6 mice in response to *L.i.* infection (Figure 1). *Cybb*, *p47*, *p67*, and *Nos2* mRNA levels were upregulated in macrophages challenged with *L.i.* (Figure 1A). In line with these results, the production of ROS and NO by macrophages following *L.i.* challenge was also strongly increased (Figures 1B and 1C).

Among the factors controlling redox balance, the transcription factor Nrf2 is a major regulator of the cellular anti-oxidant response.[5] Interestingly, the Nrf2 mRNA and protein levels, and its target genes, were upregulated during *L.i.* infection in macrophages from C57BL/6 mice (Figures 1D and 1E). This was supported by the gradual increase of Nrf2 nuclear translocation from 4 to 48 h post-*L.i.* challenge (Figure 1E) and its DNA-binding activity at 4 and 48 h post-*L.i.* challenge (Figure 1F).

It is well established that ROSs are key factors of Nrf2 activation.[6] Here, we observed that the strong induction of ROS production at 4 h after *L.i.* challenge was abolished at 24 h (Figure 1G), while Nrf2 remained activated until 48 h post-*L.i.* challenge (Figures 1E and 1F). Among the immunoregulatory mediators produced during *Leishmania* infection, PGE2 was recently identified to facilitate parasite survival.[21] Interestingly, we demonstrate here in macrophages challenged with *L.i.* a specific increase of mRNA and protein levels of COX-2 and prostaglandin E synthase (PGES); both are arachidonic acid metabolism enzymes involved in PGE2 production and EP2, a PGE2 receptor, expression (Figures 1H and 1I). Consistently, PGE2 production by macrophages was progressively increased from 4 h post-*L.i.* challenge (Figure 1J).

To establish that Nrf2 activation in macrophages is dependent on ROS during the early stages of infection and on PGE2 production at the late stages, we evaluated the DNA-binding activity of Nrf2 in macrophages pre-treated with GSK2795039 (NOX2 inhibitor) or CAY10526 (PGES inhibitor) associated with AH6808 (EP2 antagonist) (Figure 1F). Accordingly, we found that the inhibition of ROS production only reduced Nrf2 translocation at 4 h post-*L.i.* challenge, while that of the PGE2 pathway decreased Nrf2 activation at 48 h post-*L.i.* challenge (Figure 1F).

In support of these data, we employed a murine model of *L.i.* visceral infection that displayed a high concentration of urinary 8-isoprostane (reflecting oxidative stress) in the early stages post-infection (4–24 h), accompanied by a drastic decrease of urinary 8-isoprostane from 48 h post-infection and thereafter (days 7 and 15 post-infection) (Figure 1K). By contrast, the PGE2 metabolite levels in urine increased only after 48 h post-infection (Figure 1K); surprisingly, this level remained elevated until day 15 after infection. Moreover, this model also showed that the lack of ROS induction and increase of the PGE2 level was associated with the overexpression of *Ptgs2*, *Pges*, and *Ptger2* mRNA in peritoneal macrophages at day 15 post-*L.i.* infection (Figures 1L and 1M), strengthening the proposed contribution of ROS during early Nrf2 activation and the later involvement of PGE2 in the maintenance of Nrf2 activation throughout *L.i.* infection.

To dissect how PGE2 regulates Nrf2 activity, the expression of Nrf2 target genes (indicative of Nrf2 transcriptional activity) in response to *L.i.* was evaluated in the presence of specific inhibitors of signaling pathways known to activate this transcription factor[23] (Figure S1). Interestingly, the induction of HO-1, SOD1, Srxn1, and Gclm1 in response to *L.i.* was strongly decreased by PD0325 (MAPK/ERK kinase [MEK]/extracellular signal-regulated kinase [ERK] inhibitor) and skepinone (P38 mitogen-activated protein [MAP] kinase inhibitor), while treatment with staurosporin (protein kinase C [PKC] inhibitor) and H89 (protein kinase A [PKA] inhibitor) failed to modulate this gene signature. These data support the involvement of the MAP kinase signaling cascade in the PGE2-mediated Nrf2 activation upon challenge with *L.i.*

ROS- and PGE2-mediated Nrf2 activation results in opposite *Leishmania* proliferation outcomes

To evaluate the contribution of ROS- and PGE2-mediated Nrf2 activation to the control of *L.i.* proliferation by macrophages,

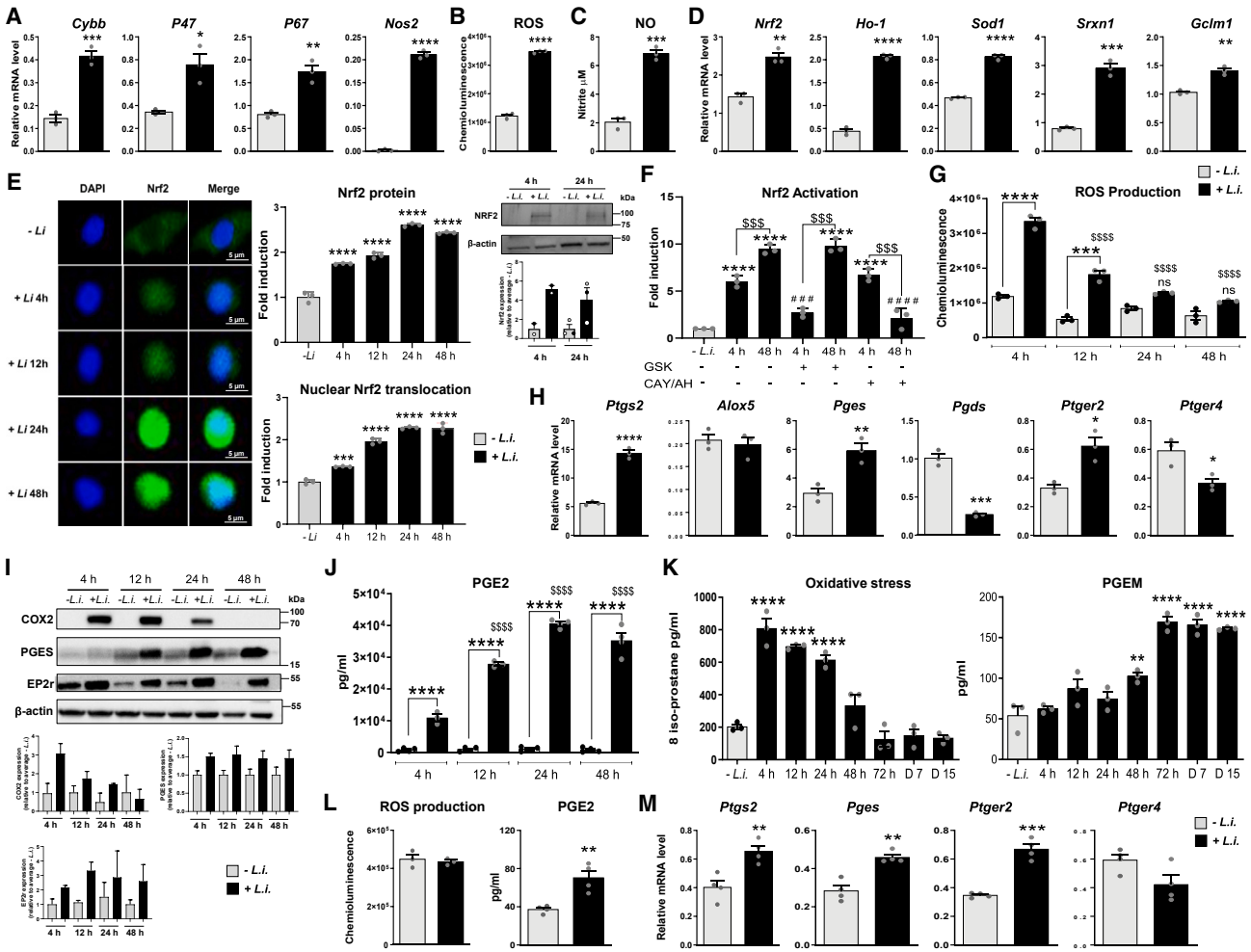

Figure 1. *L.i.* triggered ROS and PGE2 production leading to Nrf2 activation

(A–J) All analyses were performed *in vitro* on peritoneal macrophages from C57BL/6 mice in response to *L.i.* challenge. Bars represent mean values ± SEM and are representative of 3 biological replicates, each with 3 technical replicates.

(A) RT-qPCR analysis of NOX2 subunits and *Nos2* genes after 4 h of *L.i.* challenge.

(B and C) ROS (B) and NO (C) production.

(D) RT-qPCR analysis of Nrf2 and its target genes 4 h post-*L.i.* challenge.

(E) Immunofluorescence imaging of Nrf2 cellular localization (green) at 4, 12, 24, and 48 h post-infection (nuclei were stained with DAPI, blue). Scale bars, 5 µm. The top histogram represents the quantification of Nrf2 protein, and the bottom histogram represents the nuclear translocation of Nrf2, both compared to uninfected macrophages (−*L.i.*). The data are represented in a fold induction relative to uninfected peritoneal macrophages. Immunoblot analysis and quantification of Nrf2 protein after 4 and 24 h post-*L.i.* challenge (n = 2–3 experiments).

(F) DNA-binding ELISA quantification of the antioxidant responsive element (ARE)-nuclear binding of Nrf2 in peritoneal macrophages pre-treated with a NOX2 inhibitor (GSK2795039) or a prostaglandin E synthase (PGES) inhibitor (CAY10526) and an EP2 antagonist (AH6808) and infected with *L.i.* for 4 or 48 h. The data are represented in a fold induction relative to untreated and uninfected peritoneal macrophages.

(G) ROS production at 4, 12, 24, and 48 h after *L.i.* challenge.

(H) RT-qPCR analysis of arachidonic acid metabolism enzymes 4 h post-*L.i.* challenge.

(I) Immunoblot analysis and quantification of COX2, PGES, and EP2r proteins after 4, 12, 24, and 48 h post-*L.i.* challenge (n = 2–4 experiments).

(J) ELISA quantification of PGE2 production by peritoneal macrophages at 4, 12, 24, and 48 h post-*L.i.* challenge.

(K and L) C57BL/6 mice (n = 3 mice per group) were infected (i.p.) with 50 × 10^6 *L.i.* for 14 days. Bars represent mean values ± SEM (n = 3 biological replicates).

(K) Urine from infected mice was collected at 4 h, 12 h, 24 h, 48 h, 72 h, 7 days, and 14 days for determination of PGE2 and 8-isoprostane levels by ELISA.

(L) ROS and PGE2 production by peritoneal macrophages from infected mice for 14 days.

(M) RT-qPCR analysis of arachidonic acid metabolism genes 14 days after infection in peritoneal macrophages.

Significance was determined by an unpaired Student's t test (A–D, H, L, and M) or a one-way ANOVA analysis (E–G and I–K). $^{*}p < 0.05$, $^{**}p < 0.01$, $^{***}p < 0.001$, and $^{****}p < 0.0001$ compared to the uninfected macrophages (−*L.i.*). $^{\$}p < 0.05$, $^{\$\$}p < 0.01$, $^{\$\$\$}p < 0.001$, and $^{\$\$\$\$}p < 0.0001$ compared to the infected macrophages at 4 h (4 h + *L.i.*). $^{\#}p < 0.05$, $^{\#\#}p < 0.01$, $^{\#\#\#}p < 0.001$, and $^{\#\#\#\#}p < 0.0001$ compared to corresponding control (+*L.i.* 4 h untreated).

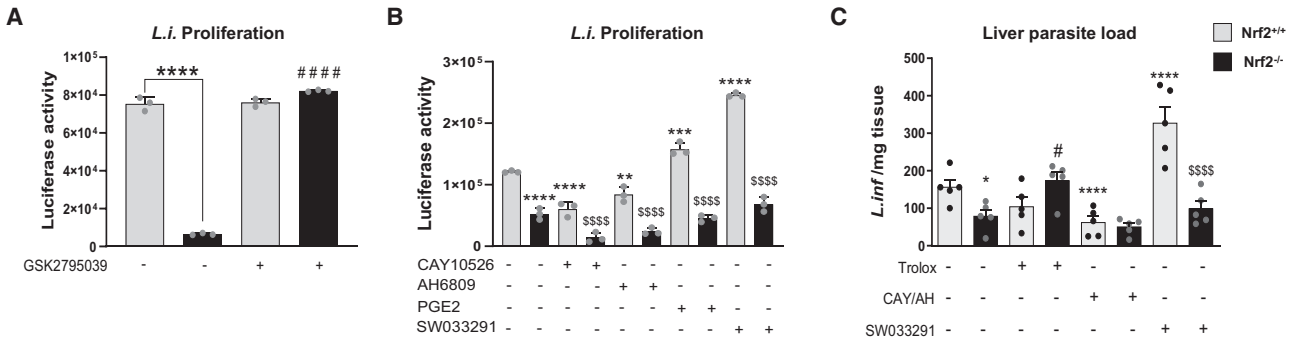

Figure 2. ROS- and PGE2-mediated Nrf2 activation promoted *L.i.* proliferation

(A and B) *L.i.* proliferation in peritoneal macrophages from $Nrf2^{+/+}$ and $Nrf2^{-/-}$ mice pre-treated with a NOX2 inhibitor (GSK2795039) (A) or PGES inhibitor (CAY10526) associated with an EP2 antagonist (AH6808), a 15-PGDH inhibitor (SW033291), or PGE2 (B). Bars represent mean values ± SEM and are representative of 3 biological replicates, each with 3 technical replicates. Significance was determined by a one-way ANOVA analysis. $^{*}p < 0.05$ and $^{****}p < 0.0001$ compared to untreated macrophages from $Nrf2^{+/+}$ mice. $^{\#\#\#\#}p < 0.0001$ compared to untreated macrophages from $Nrf2^{-/-}$ mice. $^{\$\$\$}p < 0.001$ and $^{\$\$\$\$}p < 0.0001$ compared to the respective treated macrophages from $Nrf2^{+/+}$ mice.

(C) Parasite load was quantified by RT-qPCR in $Nrf2^{+/+}$ and $Nrf2^{-/-}$ mice infected (i.p.) with 50×10^6 *L.i.* for 14 days. Mice were treated with a ROS chelator (Trolox), a cocktail of PGES inhibitor (CAY10526) and EP2 antagonist (AH6808), or a 15-PGDH inhibitor (SW033291) ($n = 5$ mice per group). Bars represent mean values ± SEM, and experiments were repeated twice. Significance was determined by a one-way ANOVA analysis. $^{*}p < 0.05$ and $^{****}p < 0.0001$ compared to the respective untreated $Nrf2^{+/+}$ mice. $^{\#}p < 0.05$ compared to untreated $Nrf2^{-/-}$ mice. $^{\$\$\$\$}p < 0.0001$ compared to the respective treated $Nrf2^{+/+}$ mice.

we examined *L.i.* proliferation in macrophages deficient for Nrf2 ($Nrf2^{-/-}$). As expected, *L.i.* proliferation was prevented in macrophages lacking Nrf2, while the inhibition of ROS production by GSK2795039 reciprocally restored *L.i.* proliferation in $Nrf2^{-/-}$ macrophages (Figure 2A). Likewise, the inhibition of PGE2 production with CAY10526 (PGES inhibitor) and treatment with AH6808 (EP2 receptor antagonist) both decreased *L.i.* proliferation only in $Nrf2^{+/+}$ macrophages, whereas the exogenous addition of PGE2 reciprocally increased *L.i.* proliferation (Figure 2B). In parallel, treatment of $Nrf2^{+/+}$ and $Nrf2^{-/-}$ macrophages with SW033291, a 15 PGDH inhibitor (enzyme of PGE2 degradation), increased *L.i.* proliferation only in those cells expressing this transcriptional factor (Figure 2B), thus demonstrating that the impact of Nrf2 in promoting *L.i.* proliferation involved specifically the PGE2/EP2 axis.

In line with this, the parasite load in the liver was lower in $Nrf2^{-/-}$ mice infected by *L.i.* (Figure 2C). As expected, treatment with Trolox (ROS chelator) increased the number of *L.i.* in the liver of $Nrf2^{-/-}$ mice but not that of the control counterpart (Figure 2C). Interestingly, loss of function of PGE2 production by CAY10526/AH6808 reduced significantly the number of *L.i.* in the liver of $Nrf2^{+/+}$ mice (Figure 2C), while gain of function of this lipid mediator through SW033291 treatment strongly increased the parasite load in the liver of $Nrf2^{+/+}$ mice only (Figure 2C). Altogether, these data demonstrate that ROS and the PGE2/EP2 axis mediate Nrf2 activation to promote *L.i.* growth.

Nrf2 in macrophages promotes *L.i.* infection through the induction of an anti-oxidant and anti-inflammatory phenotype

As the parasite load in the liver and spleen was significantly decreased in $Nrf2^{-/-}$ mice compared to their infected wild-type littermates (Figures 2C and 3A), we dissected how Nrf2 in macrophages promotes *L.i.* infection in our visceral murine model of leishmaniasis. To this end, we evaluated *ex vivo* the ability of peritoneal macrophages from $Nrf2^{+/+}$ and $Nrf2^{-/-}$ mice to engulf and control the proliferation of *L.i.* (Figures 3B–3D). Although there was no difference in the phagocytosis capacity between macrophages from $Nrf2^{+/+}$ and $Nrf2^{-/-}$ mice, the proliferation of *L.i.* was decreased in macrophages from $Nrf2^{-/-}$ mice (Figures 3B and 3C). Interestingly, the ROS and NO production of macrophages from infected $Nrf2^{-/-}$ mice was increased in response to *L.i.* challenge compared to macrophages from infected $Nrf2^{+/+}$ mice (Figure 3D). In line with this, the mRNA expression of *Cybb*, *P47*, and *Nos2* was upregulated in macrophages from infected $Nrf2^{-/-}$ mice, whereas the *Arg-1* mRNA level was downregulated in these cells (Figure 3E). Further analyses of the gene expression and protein level of cytokines in macrophages from $Nrf2^{+/+}$ and $Nrf2^{-/-}$ infected mice revealed a significant increase of interleukin (IL)-β, IL-12, tumor necrosis factor alpha (TNF-α), and IL-6 pro-inflammatory signals in cells deficient for Nrf2, which was mirrored by a decrease of IL-10 and transforming growth factor beta (TGF-β) anti-inflammatory factors (Figure 3F). Consistent with the pro-inflammatory profile of $Nrf2^{-/-}$ macrophages, the mRNA levels of *Fcgr3a*, *Fcgr2b*, *Itgam*, and *Ccr2,* were also increased in these cells (Figure 3G). Collectively, these data demonstrate that Nrf2 tilts macrophages toward an anti-inflammatory and anti-oxidant phenotype, enabling the progression of *L.i.* infection.

As a proof of principle that Nrf2 of macrophages is required for *L.i.* resilience, we performed an adoptive transfer (AT) of $Nrf2^{-/-}$ macrophages into infected $Nrf2^{+/+}$ recipient mice (Figure 3H). AT resulted in a decrease of the parasite load in the liver while simultaneously supporting an increase of microbicidal functions such as ROS, as reflected by the 8-isoprostane production and NO and cytokine production in the peritoneal cavity, reminiscent of the effect observed in infected $Nrf2^{-/-}$ mice (Figure 3H). Therefore, Nrf2 expression in macrophages likely promotes systemic vulnerability to *L.i.* infection.

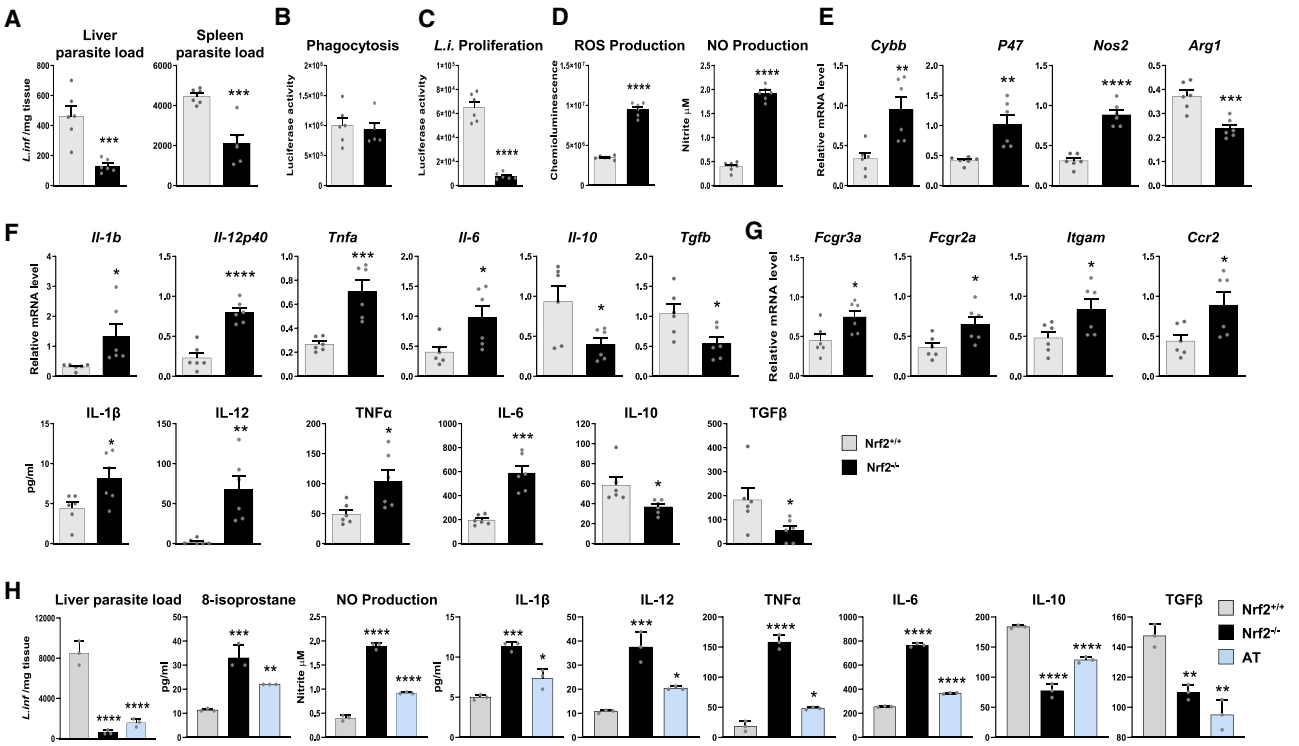

Figure 3. Nrf2 promotes *L.i.* infection in macrophages via an anti-oxidant and anti-inflammatory phenotype

(A–G) *Nrf2*$^{+/+}$ and *Nrf2*$^{-/-}$ mice (n = 6 mice per group) were infected (i.p.) with 50 × 10^6 *L.i.* for 14 days. Bars represent mean values ± SEM, and experiments were repeated three times.

(A) Parasite loads in liver and spleen were quantified by RT-qPCR.

(B–D) *Ex vivo* phagocytosis (B) and proliferation of *L.i.* (C) in peritoneal macrophages and ROS and NO (D) production by peritoneal macrophages from *Nrf2*$^{+/+}$ and *Nrf2*$^{-/-}$ mice.

(E–G) RT-qPCR and ELISA analysis on peritoneal macrophages from *in-vivo*-infected *Nrf2*$^{+/+}$ and *Nrf2*$^{-/-}$ mice of oxidative stress markers (E), cytokines (F), and surface receptors (G).

(H) An adoptive transfer (AT) of *Nrf2*$^{-/-}$ macrophages (n = 9 mice) into *Nrf2*$^{+/+}$ recipient mice (n = 3 mice) was performed before *L.i.* infection for 14 days. 8-Isoprostane, NO production, and cytokine secretion were measured in peritoneal fluids. Bars represent mean values ± SEM, and experiments were repeated twice.

Significance was determined by an unpaired Student's t test (A–F) except for (H), where significance was determined by a one-way ANOVA analysis. *p < 0.05, **p < 0.01, ***p < 0.001, and ****p < 0.0001 compared to infected *Nrf2*$^{+/+}$ mice.

The expression of Nrf2 in macrophages prevents the death of *L.i.* by lipid peroxidation

To dissect how *L.i.* is eliminated in *Nrf2*$^{-/-}$ mice, we next evaluated whether the decrease in parasite proliferation was due indirectly to an enhanced macrophage microbicidal capacity or directly to a reduction in parasite fitness. We first confirmed *in vitro* that there was no difference in the cell viability of *Nrf2*$^{+/+}$ and *Nrf2*$^{-/-}$ macrophages infected with *L.i.* (Figure 4A). Given the case, we then turned to the literature, where it has been recently described that the accumulation of oxidative stress induced the peroxidation of polyunsaturated fatty acids, an essential step of ferroptosis. In addition, GPX4, a critical anti-ferroptotic enzyme, has been annotated as a *bona fide* target gene of Nrf2.[24] Within this context, we consequently evaluated whether *L.i.* died by ferroptosis in *Nrf2*$^{-/-}$ macrophages. To accomplish this, we measured the lipid peroxidation of *L.i.* using C11-BODIPY, a redox-sensitive dye, in *Nrf2*$^{+/+}$ and *Nrf2*$^{-/-}$ macrophages (Figure 4B), and the number of living *Leishmania* in macrophages was estimated through their luciferase activity (Figure 4C). We observed higher lipid peroxidation of *L.i.* in *Nrf2*$^{-/-}$ macrophages (Figure 4B), which was associated with a decrease of the *L.i.* number (Figure 4C). Interestingly, the addition of ferrostatin-1 (Fe-1), an inhibitor of ferroptosis, prevented *L.i.* lipid peroxidation in *Nrf2*$^{-/-}$ macrophages, diminishing their capacity to control the *L.i.* number (Figure 4C). These results were supported by an increased peroxidation of *L.i.* lipids associated with a drastic decrease in the number of *L.i.* in *Nrf2*$^{+/+}$ and *Nrf2*$^{-/-}$ macrophages following treatment with cumene hydroperoxide (CuOOH), a ferroptosis inducer (Figure 4C). These findings suggested that Nrf2-induced ROS inhibition protected *L.i.* from a microbicidal process highly resembling ferroptosis.

To confirm that ROS was responsible for *L.i.* lipid peroxidation and death, we studied the *in vitro* lipid peroxidation and viability of *L.i.* in the presence of H_2O_2, a non-ROS radical (Figures 4D and 4E). In the presence of H_2O_2, *L.i.* lipid peroxidation was strongly induced, and *L.i.* viability was impaired. The addition of Fe-1 protected *L.i.* from H_2O_2-induced lipid peroxidation

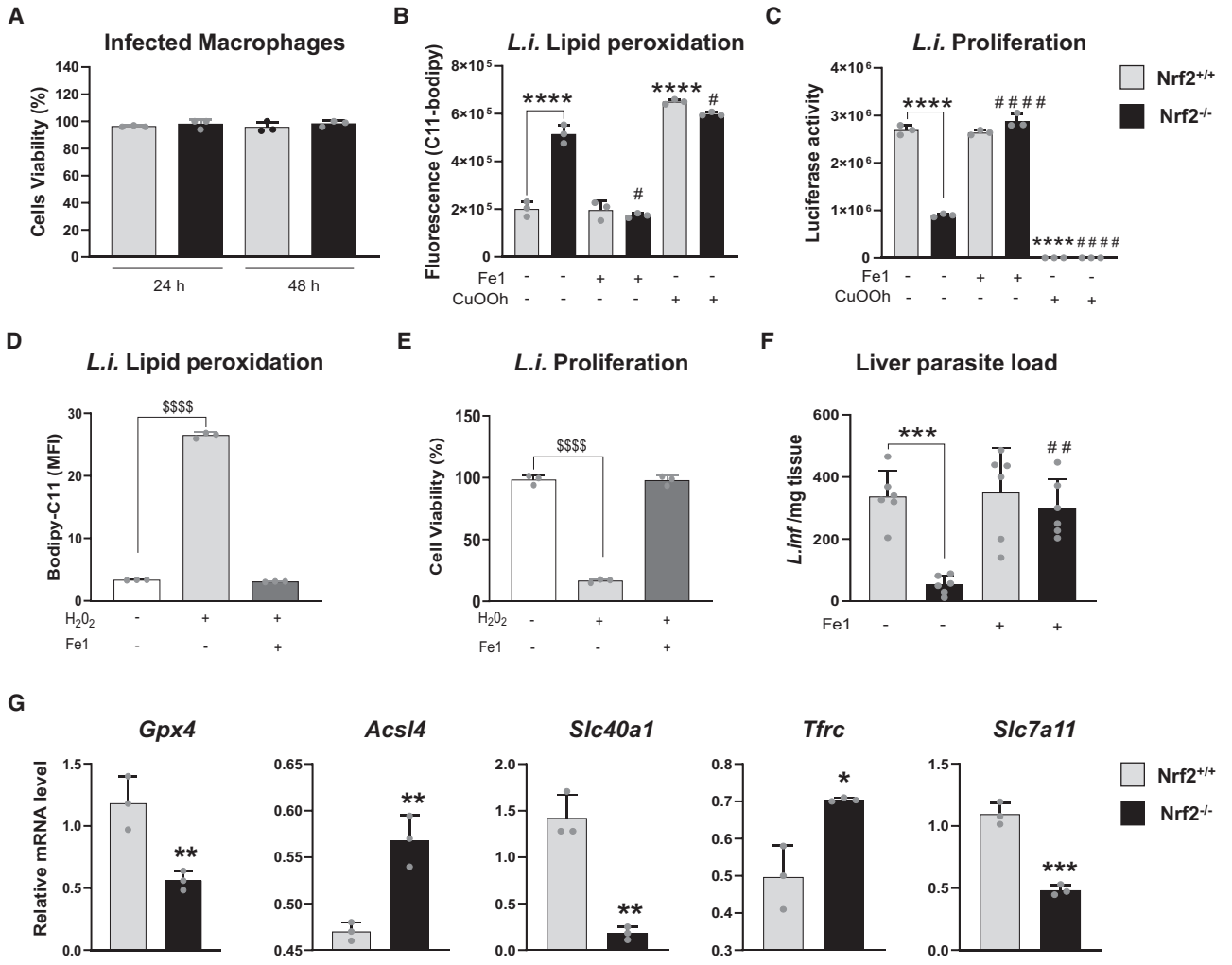

Figure 4. Nrf2 expression in macrophages prevents the death of *L.i.* by ferroptosis

(A–E) Bars represent mean values ± SEM and are representative of 3 biological replicates, each with 3 technical replicates.

(A) Viability of peritoneal macrophages from *Nrf2*$^{+/+}$ and *Nrf2*$^{-/-}$ mice infected with *L.i.* for 24 and 48 h.

(B and C) Quantification of *L.i.* lipid peroxidation (B) and *L.i.* proliferation (C) in peritoneal macrophages from *Nrf2*$^{+/+}$ and *Nrf2*$^{-/-}$ mice treated with ferrostatin-1 (Fe-1) or cumene hydroperoxide (CuOOH).

(D) Quantification of lipid peroxidation in *L.i.* promastigotes treated (or not) with H_20_2 for 4 h and Fe-1.

(E) Quantification of *L.i.* proliferation treated (or not) with H_20_2 for 4 h and Fe-1.

(F) Parasite load was quantified by RT-qPCR in *Nrf2*$^{+/+}$ and *Nrf2*$^{-/-}$ mice infected (i.p.) with 50 × 10^6 *L.i.* for 14 days and treated or not with Fe-1 ($n = 6$ per group).

(G) RT-qPCR analysis of ferroptosis markers on peritoneal macrophages from infected *Nrf2*$^{+/+}$ and *Nrf2*$^{-/-}$ mice treated or not with Fe-1. The experiment was repeated twice.

Significance was determined by a one-way ANOVA analysis (A–F) except for (G), where significance was determined by an unpaired Student's t test. $^{****}p < 0.0001$ compared to untreated peritoneal macrophages from *Nrf2*$^{+/+}$ mice. $^{\#}p < 0.05$ and $^{\#\#\#\#}p < 0.0001$ compared to untreated peritoneal macrophages from *Nrf2*$^{-/-}$ mice. $^{\$\$\$\$}p < 0.0001$ compared to untreated *L.i.* promastigotes.

and improved their viability (Figures 4D and 4E). Finally, we infected *Nrf2*$^{+/+}$ and *Nrf2*$^{-/-}$ mice with *L.i.* in the presence or absence of Fe-1. Given the very low persistence of Fe-1, mice were treated each day with Fe-1. We observed that the decrease in parasite load displayed by the *Nrf2*$^{-/-}$ mice was completely abolished with Fe-1 treatment (Figure 4F), thus suggesting that host-driven ferroptosis-like process is a critical mechanism of defense against *L.i.* at the cellular and systemic levels.

Altogether, these results argue that Nrf2 in macrophages protects *L.i.* from lipid peroxidation, preventing their death by a mechanism reminiscent of ferroptosis. These findings are further supported by the downregulation of *Gpx4*, *Slc40a1*, and *Slc7a11* genes (negative regulators of ferroptosis) and, conversely, an upregulation of *Acsl4* and *Tfrc* genes (positive regulators of ferroptosis) in macrophages from Nrf2-deficient mice (Figure 4G).

Pharmacological inhibition of Nrf2 reduces *L.i.* infection through an oxidative and inflammatory profile of macrophages

To validate Nrf2 as a relevant therapeutic target for visceral leishmaniasis treatment, we used a pharmacological inhibitor of Nrf2, such as ML-385, in mice infected with *L.i.* (Figure 5). Strikingly, 15 days after infection, the parasite loads in the spleen and liver of infected mice were decreased in a similar fashion to when the mice were treated either with ML385 or liposomal amphotericin B (AmB), a standard treatment for visceral leishmaniasis (Figure 5A). Likewise, the proliferation of *L.i.* was decreased in macrophages from infected mice treated with ML385, suggesting that the pharmacological inhibition of Nrf2 promoted the microbicidal function of macrophages (Figure 5B). Consistent with these observations, the ML385 treatment of infected mice also increased the ROS and NO production of macrophages in response to *L.i.* challenge (Figures 5C and 5D). In addition, the lipid peroxidation of *L.i.* in macrophages was significantly induced by ML385 treatment (Figure 5E); this treatment also upregulated the mRNA and protein levels of IL-β, IL-12, TNF-α, and IL-6 pro-inflammatory cytokines and downregulated the IL-10 anti-inflammatory cytokine (Figure 5F). Therefore, these data obtained through a pharmacological approach argue in favor of the therapeutic potential of Nrf2 modulation in the treatment of visceral leishmaniasis.

The involvement of Nrf2 in *Leishmania* infection and its potential as a therapeutic target was strengthened by the comparison of the progression of *L.i.* infection between susceptible (C57BL/6) and resistant (129/Sv) mouse strains (Figures 5G–5K). As expected, the parasite burdens in the liver and spleen were notably lower in 129/Sv mice compared to those from the C57BL/6 background (Figure 5G). Moreover, while the ML385 treatment resulted in a moderate decrease of the parasite loads in the spleen and liver of infected 129/Sv mice, C57BL/6 mice displayed a drastic reduction in these readouts at 15 days post-infection (Figure 5G). At the cellular level, the proliferation of *L.i.* was diminished in macrophages derived from infected 129/Sv mice compared to those from C57BL/6 mice (Figure 5H). Similar to the global effect in mice from different backgrounds, the ML385 treatment slightly reduced *L.i.* proliferation in 129/Sv macrophages compared to its strong diminishing effect on cells from C57BL/6 mice (Figure 5H). Interestingly, unlike macrophages from C57BL/6 mice, which exhibited a significant upregulation of mRNA expression for Nrf2 along with its target genes during *L.i.* infection, 129/Sv macrophages displayed no gene modulation (albeit a minor induction of *Ho-1* and *Srxn1*) (Figures 5I and 5J). This gene modulation pattern was further reflected in the Nrf2 DNA-binding activity observed at 4 h post-*L.i.* challenge, whose increase was evident only in C57BL/6 macrophages (Figure 5K). In summary, these findings unequivocally demonstrate differences (at the global and cellular levels) in *L.i.* proliferation, Nrf2 activation, and binding to its specific nucleotide sequence upon *L.i.* challenge, according to the mouse background.

ROS/PGE2-axis-mediated Nrf2 activation enables *L.i.* proliferation in h-MDMs

To validate our findings obtained through the use of a murine model within the human context, we challenged human monocyte-derived macrophages (h-MDMs) with *L.i.* (Figure 6). First, the mRNA and protein levels of Nrf2 and its target genes (HO-1, SRXN1, NQ01) in h-MDM were strongly increased by *L.i.* challenge (Figure 6A). Second, similar to our findings in the murine model, the *CYBB* and *P47* mRNA levels were upregulated in h-MDMs challenged with *L.i.* (Figure 6B). In line with this, the production of ROSs by h-MDMs following *L.i.* challenge was increased during the early stage of infection (4 h), followed by a gradual decrease as a function of time (Figure 6C); conversely, PGE2 production by h-MDMs was progressively increased from 4 h post-*L.i.* challenge (Figure 6E). Consistent with this increased PGE2 production, *PTGS2*, *PGES*, and *PTGER2* mRNA levels were also upregulated following *L.i.* challenge, while *PGDS* and *PTGER4* were downregulated (Figure 6D). Consequently, Nrf2 nuclear translocation in h-MDMs was gradually increased from 4 to 48 h post-*L.i.* challenge (Figure 6F).

To continue our validation concerning the dynamics of Nrf2 activation by ROS and PGE2 during the early and late stages of *L.i.* infection, respectively, we evaluated its nuclear translocation in h-MDMs pre-treated with GSK2795039 (NOX2 inhibitor) or CAY10526 (PGES inhibitor), associated with AH6808 (EP2 antagonist) (Figure 6G). As expected, Nrf2 translocation was reduced by GSK2795039 only at 4 h post-*L.i.* challenge and, subsequently, by CAY10526/AH6808 only at 48 h post-*L.i.* challenge (Figure 6G). As a result, *L.i.* proliferation was increased in h-MDMs by GSK2795039 treatment or exogenous PGE2 delivery; the inhibition of PGE2 production by CAY10526/AH6808, however, reduced *L.i.* proliferation (Figure 6H), confirming the contribution of the ROS- and PGE2-mediated Nrf2 activation to the control of *L.i.* proliferation by h-MDMs. Furthermore, the pharmacological inhibition of Nrf2 by ML385 abrogated *L.i.* proliferation in h-MDMs (Figure 6I). Consistent with the anti-proliferative effect of ML385, *L.i.* lipid peroxidation and 8-isoprostane, ROS, and NO production were strongly increased in infected h-MDMs treated with ML385 (Figures 6J–6M).

Altogether, these data argue that the ROS/PGE2 axis mediates Nrf2 activation to control *L.i.* proliferation in the context of human macrophages.

DISCUSSION

Leishmania parasites have developed clever strategies to resist various microbicidal mechanisms, including the oxidative burst generated by the host macrophages to limit parasite growth, upon entering host cells. Here, we demonstrated that an increase in ROS production by murine and human macrophages during the early stages of *L.i.* infection leads to the efficient control of parasite proliferation. The use of a pharmacological inhibitor of the NADPH oxidase (NOX2) reduced Nrf2 nuclear translocation in murine and human macrophages, strengthening the contribution of ROS in the early Nrf2 activation. Consistently, *L. guyanensis* was recently shown to mediate the activation of NADPH oxidase leading to the release of Nrf2 from its negative regulator KEAP1, thus enabling its translocation of Nrf2 into the nucleus.[13]

During the early stages of *L.i.* infection, this study reports a counteracting dual role for ROSs. On the one hand, ROSs are

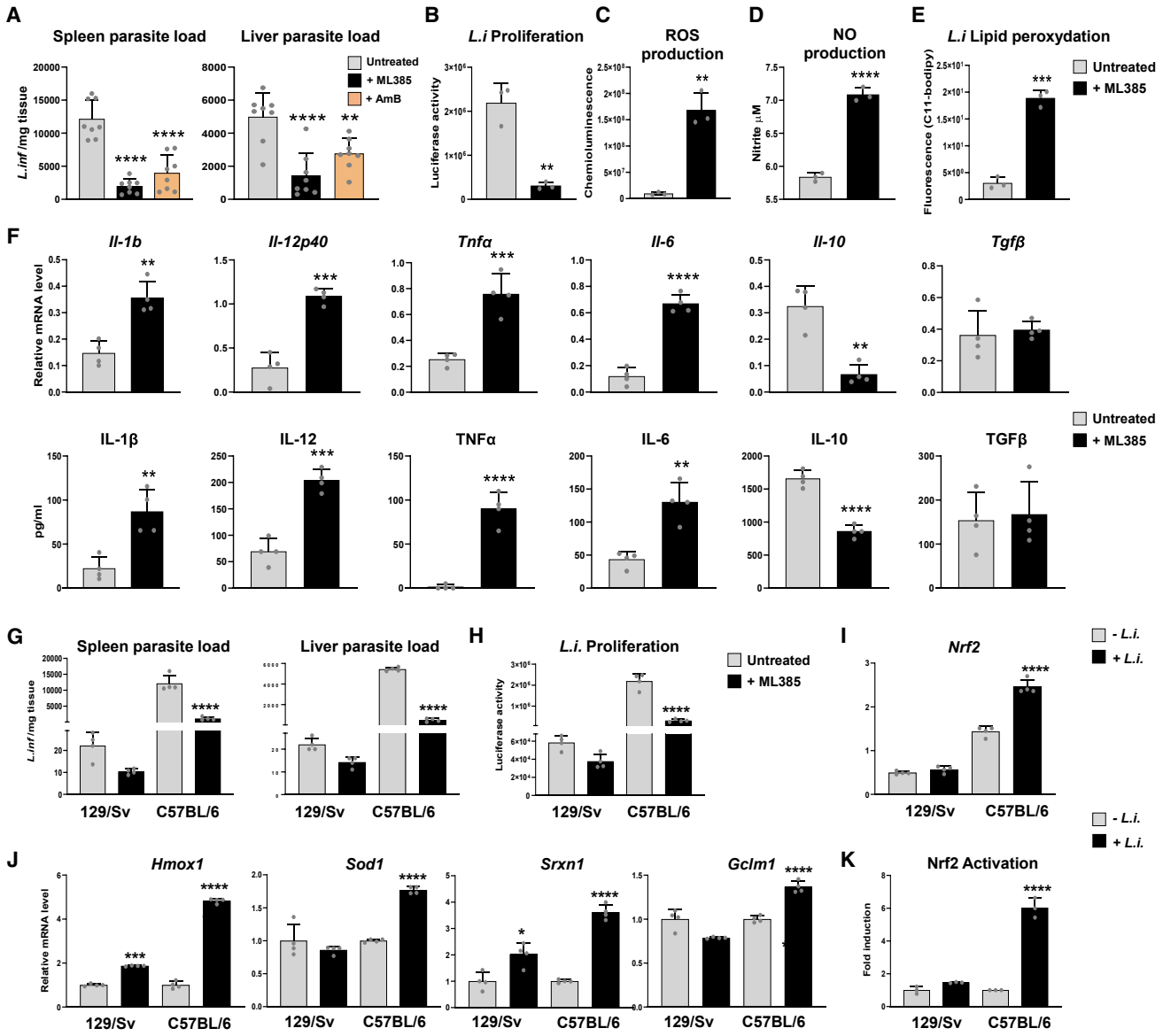

Figure 5. Pharmacological inhibition of Nrf2 reduces *L.i.* infection through an oxidative and inflammatory profile in macrophages

(A–F) C57/BL6 mice were infected (i.p.) with 50 × 10^6 *L.i.* for 14 days and treated (or not) with ML385 (Nrf2 inhibitor) or liposomal amphotericin B (AmB) (n = 8 mice per group).

(A) Parasite loads in liver and spleen were quantified by RT-qPCR.

(B) *L.i.* proliferation in peritoneal macrophages.

(C and D) ROS (C) and NO (D) production by peritoneal macrophages.

(E) *Ex vivo* quantification of *L.i.* lipid peroxidation in peritoneal macrophages.

(F) RT-qPCR and ELISA analysis of cytokines on peritoneal macrophages.

(G and H) 129/Sv mice (n = 4 mice per group) were infected (i.p.) with 50 × 10^6 *L.i.* for 14 days, treated (or not) with ML385 (Nrf2 inhibitor), and compared to data from C57/BL6 mice infected with *L.i.*

(G) Parasite loads in liver and spleen were quantified by RT-qPCR.

(H) *L.i.* proliferation in peritoneal macrophages.

(I and J) RT-qPCR analysis of Nrf2 (I) and its target genes (J) on peritoneal macrophages from 129/Sv and C57/BL6 mice infected with *L.i.*

(K) DNA-binding ELISA quantification of the ARE-nuclear binding of Nrf2 in peritoneal macrophages from 129/Sv and C57/BL6 mice infected with *L.i.* The data are represented in a fold induction relative to untreated and uninfected peritoneal macrophages. Bars represent mean values ± SEM from 3 biological replicates, each with 3 technical replicates. Significance was determined by a one-way ANOVA analysis. $^{**}p < 0.01$, $^{***}p < 0.001$, and $^{****}p < 0.0001$ compared to untreated mice.

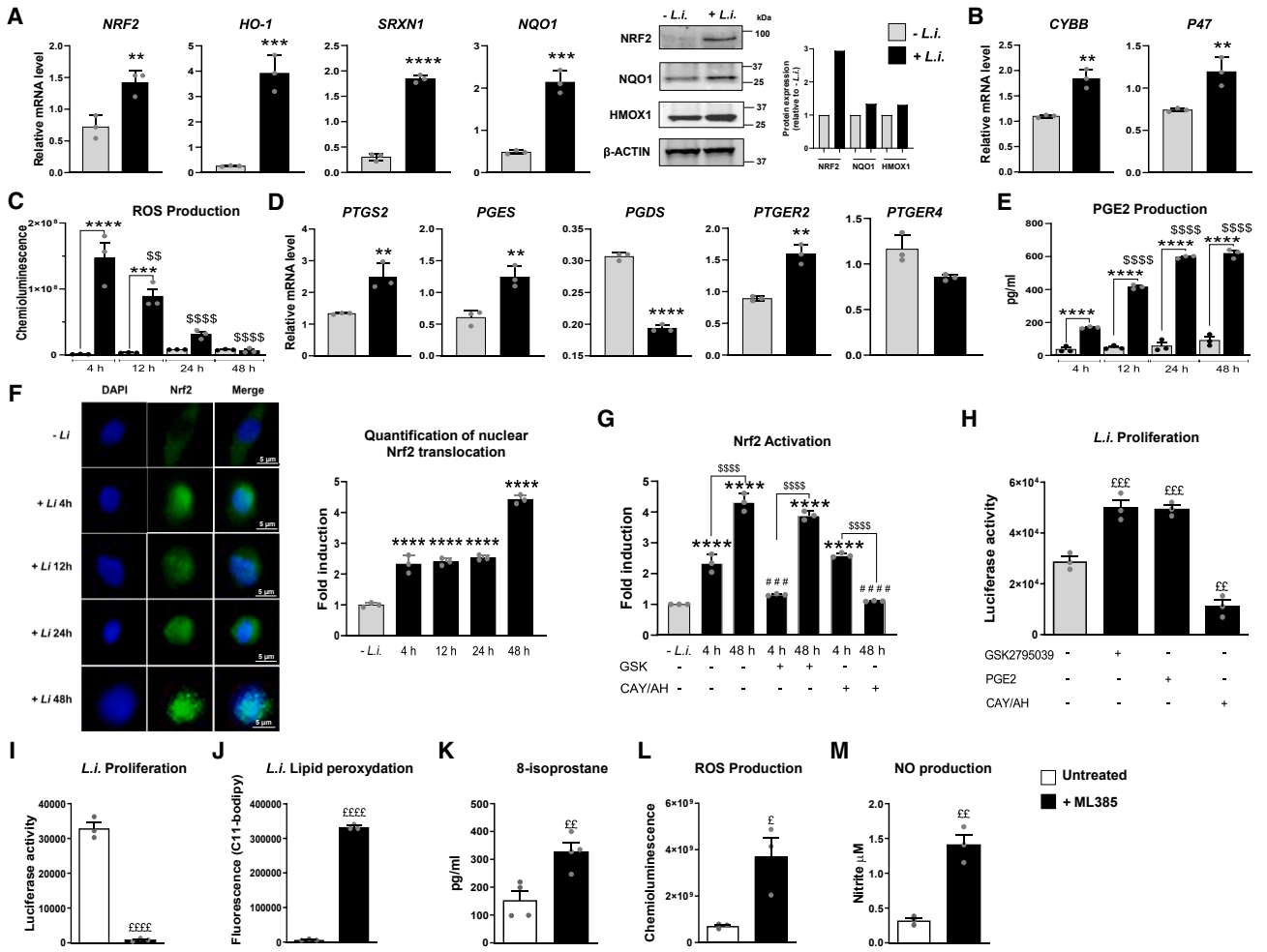

Figure 6. ROS/PGE2-axis-mediated Nrf2 activation enables *L.i.* proliferation in h-MDMs

(A–M) All analyses were performed *in vitro* on human monocyte-derived macrophages (h-MDMs) in response to *L.i.* challenge.

(A) RT-qPCR analysis, immunoblots, and quantification of NRF2 and its target genes after *L.i.* challenge.

(B) RT-qPCR analysis of NADPH oxidase subunits at 4 h after *L.i.* challenge.

(C) ROS production at 4, 12, 24, and 48 h after *L.i.* challenge.

(D) RT-qPCR analysis of arachidonic acid metabolism genes 4 h after *L.i.* challenge.

(E) PGE2 production by h-MDMs at 4, 12, 24, and 48 h after *L.i.* challenge.

(F) Immunofluorescence imaging of NRF2 cellular localization (green) and DAPI-labeled nucleus (blue) at 4, 12, 24, and 48 h after *L.i.* challenge. Quantification of the nuclear translocation of NRF2 compared to uninfected h-MDMs (−*L.i.*). The data are represented in a fold induction relative to uninfected h-MDMs. Scale bars, 5 µm.

(G) Quantification of nuclear translocation of NRF2 by confocal imaging (as in F) at 4 and 48 h after *L.i.* challenge in h-MDMs treated (or not) with GSK2795039 (NOX2 inhibitor) or CAY10526 (PGES inhibitor) and AH6808 (EP2 antagonist). The data are represented in a fold induction relative to uninfected h-MDMs.

(H) *L.i.* proliferation in h-MDMs treated (or not) with GSK2795039, CAY10526 and AH6808, or PGE2.

(I) *L.i.* proliferation in h-MDMs treated (or not) with ML385.

(J) Lipid peroxidation of *L.i.* in h-MDMs treated (or not) with ML385.

(K) 8-Isoprostane quantification in the culture supernatant of *L.i.*-challenged h-MDMs treated (or not) with ML385.

(L and M) ROS (L) and NO (M) production by h-MDMs challenged with *L.i.* and treated (or not) with ML385. Bars represent mean values ± SEM and are representative of 3 biological replicates, each with 3–4 technical replicates.

Significance was determined by an unpaired Student's t test (A, B, D, and I–M) except for (C) and (F–H), where significance was determined by a one-way ANOVA analysis. $^{*}p < 0.05$, $^{**}p < 0.01$, and $^{****}p < 0.0001$ compared to uninfected h-MDM (−*L.i.*). $^{\$\$\$\$}p < 0.0001$ compared to 4 h infected h-MDMs (4 h + *L.i.*). $^{\#\#\#}p < 0.001$ and $^{\#\#\#\#}p < 0.0001$ compared to untreated infected h-MDMs at 4 h. $^{£}p < 0.05$, $^{££}p < 0.01$, $^{£££}p < 0.001$, and $^{££££}p < 0.0001$ compared to untreated h-MDMs (−ML385).

involved in the direct elimination of the parasite, as demonstrated in Nrf2-deficient mice. On the other hand, Trolox (ROS inhibitor) treatment led to an increase in *L.i.* proliferation. This apparent conundrum is explained by the presence of Nrf2. Indeed, the ROSs released by *L.i.* infection activate Nrf2 that subsequently triggers the anti-oxidant genes, which in turn

reduce ROS production and promote *L.i*. proliferation. Therefore, during the early stages of infection (4 h), ROSs contribute to the elimination of *L.i*. but simultaneously activate Nrf2 as a negative-feedback loop to regulate its production. This is confirmed in Nrf2-deficient mice, where only the leishmanicidal activity of ROSs is evident in an uncontrolled manner.

Following the kinetics analysis of *L.i.* infection revealed a sustained activation of Nrf2 that coincides with the gradual decrease of ROS production over time, suggesting an alternative mechanism for Nrf2 activation at the late stages of infection. Interestingly, and in agreement with the study of Saha et al.,[21] we identified PGE2 as the responsible factor for this late phenomenon. Indeed, we demonstrated that *L.i.* enhances COX-2 and PGES gene expression in murine and human macrophages, which in turn increases the production of PGE2. If the PGE2 synthase and the EP2 receptor are pharmacologically inhibited during the late stages of infection, then Nrf2 nuclear translocation is drastically decreased in murine and human macrophages. This strengthens the role of the COX-2/PGES/PGE2/EP2r axis to maintain Nrf2 activation throughout infection. The increase in parasite load in mice treated with the inhibitor of 15-PGDH, a PG-degrading enzyme,[25] reinforces the importance of this signaling pathway and the crucial contribution of PGE2 via EP2r, but not its metabolites, in the progression of infection. Collectively, our data show the contribution of the NOX2/ROS axis in the early activation of Nrf2 and the subsequent involvement of PGE2/EP2r in sustaining this activation upon *L.i.* infection. These data were also supported in a murine model of *L.i.* visceral infection, where we demonstrated a high concentration of urinary isoprostane, which reflects the oxidative stress, during the early stages post-infection, while the PGE2 metabolite levels in urine only increased at the later stages.

The genetic deletion of Nrf2 in *L.i.*-infected mice identified this transcription factor as a central factor in the progression of visceral leishmaniasis, particularly through its role in controlling inflammation and oxidative balance. Indeed, the parasite loads in the liver and spleen were significantly reduced in *Nrf2*$^{-/-}$ infected mice. *L.i.* clearance was related to a pro-inflammatory and pro-oxidant phenotype of macrophages, demonstrating that Nrf2 skews macrophages toward an anti-inflammatory and anti-oxidant profile that promoted the progression of *L.i*. infection. Consistent with these observations, besides the anti-oxidant role of Nrf2,[5] a recent study described an important role for Nrf2 in the suppression of the macrophage inflammatory response by blocking pro-inflammatory cytokine transcription.[26] In fact, the AT of *Nrf2*$^{-/-}$ macrophages into infected *Nrf2*$^{+/+}$ recipient mice ameliorated the host response to infection, which likely interfered with the Nrf2-induced anti-inflammatory and anti-oxidant macrophages that potentially cause the systemic vulnerability of *L.i.* infection.

Similar to the data obtained with *Nrf2*$^{-/-}$ mice, the pharmacological inhibition of Nrf2 by the administration of ML385 in infected mice reduced the parasite loads in the liver and spleen, and it also oriented the phenotype of macrophages toward a microbicidal pro-inflammatory and pro-oxidant profile. Interestingly, the evaluation of the effect of ML385 on the infection course compared to the reference treatment AmBisome[27] showed similar effects of the two molecules, highlighting the potential of ML385 for the treatment of visceral leishmaniasis.

Currently, the cell death programs of the *Leishmania* genus remain poorly defined. There is a handful of data suggesting apoptosis as a potential type of death in *Leishmania* spp. However, key apoptotic proteins involved in mammalian apoptosis have not been reported in the *Leishmania* genus.[28] In this work, we show that ROS-induced lipid peroxidation leads to a decrease in *L.i.* viability, suggesting that ferroptosis could be one type of death program present in *Leishmania*. In this context, it was recently demonstrated in *Trypanosoma brucei*, a parasite belonging to the *Trypanosomatidae* family like *Leishmania* species, that its death could also involve ferroptosis upon lipid peroxide accumulation.[19] To further support the occurrence of ferroptosis in *L.i.*, here we demonstrated that *L.i.* infection in macrophages that genetically invalidated, or pharmacologically inhibited, the Nrf2 activity induced an oxidative burst leading to lipid peroxidation of parasites and their death. Therefore, the anti-oxidant effect of Nrf2 in macrophages protected *L.i.* against lipid peroxidation and the ferroptosis death program. How Nrf2 activity in macrophages regulates the lipid peroxidation of *Leishmania* constitutes an intriguing avenue that is currently under investigation.

While targeting the Nrf2 pathway in leishmaniasis presents an interesting therapeutic angle, the study's limitations underscore the need for a more comprehensive understanding of the role of Nrf2 across different host cells and in the context of the diverse species of *Leishmania*. Broadening the research to include various immune cells and human tissue models, alongside comparative studies across different forms of leishmaniasis, would provide a more robust foundation for evaluating Nrf2 inhibition as a therapeutic strategy.

In conclusion, *L.i.* infection induces the successive production of ROS and PGE2 by macrophages leading to the activation of Nrf2 (Figure 7). This activation is responsible for the onset of an anti-oxidant and anti-inflammatory phenotype in macrophages favoring the progression of visceral leishmaniasis. In addition, we identify a ferroptosis-like cell death program of *L.i.* and the protective effect of Nrf2 activity in macrophages against this parasite's death. Finally, we highlight Nrf2 as a critical factor for the susceptibility of *L.i.* infection. Synthetic inhibition of Nrf2 activity may, hence, constitute promising compounds for the treatment of visceral leishmaniasis.

Limitations of the study

In this study, we showed that *L.i*. exploits macrophage transcription factor Nrf2 to promote its resilience within the host. To demonstrate the activation of Nrf2 in response to *L.i.*, we quantified this transcription factor specifically in the nucleus by immunofluorescence. Moreover, the evaluation of Nrf2 DNA-binding activity post-*L.i*. challenge, mirroring its nuclear translocation has allowed us to demonstrate that *L.i.* challenge induced Nrf2 nuclear translocation. However, due to the lack of specificity of our antibodies directed against Nrf2, we had difficulty identifying Nrf2 in the nuclear fraction by western blot. Thus, it will be necessary to assess other clones in future experiments. We also propose the pharmacological inhibition of Nrf2 for therapeutic

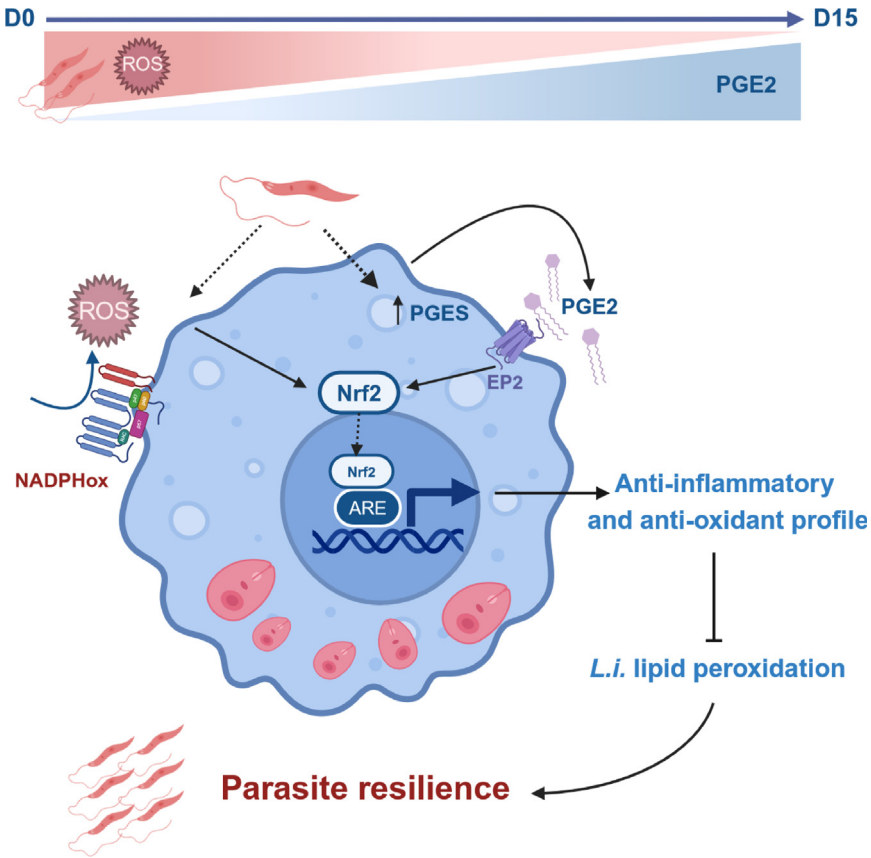

Figure 7. Schematic illustration of the ROS- and PGE2-mediated Nrf2 activation in macrophages leading to an increased resilience of *L.i*

L.i. infection induces the successive contribution of the NOX2/ROS axis in early Nrf2 activation and PGE2/EP2r signaling in the sustainment of Nrf2 activation. This activation is responsible for the onset of an anti-oxidant and anti-inflammatory phenotype in macrophages favoring the progression of visceral leishmaniasis. In addition, we establish a macrophage-driven ferroptosis-like process as a cell death program of *L.i.* and the protective effect of Nrf2 in macrophages against *L.i.* killing.

purposes in leishmaniasis, using mouse models and specifically targeting macrophages in humans. Leishmaniasis is a complex tropical disease present in various forms, which affects multiple internal organs and can be fatal if untreated. The disease's complexity is compounded by the diversity of *Leishmania* species involved, each with potentially different pathogenesis and immune evasion strategies. In our study, we used *L.i*. as a critical model for studying visceral leishmaniasis. Our study does not consider the diversity of *L.i*. strains, and whether our findings can be applicable to cutaneous leishmaniasis remains to be elucidated. Finally, Nrf2 plays a protective role in cells by regulating the expression of anti-oxidant enzymes and detoxifying proteins. Its inhibition, particularly in the context of an infectious disease like leishmaniasis, which involves oxidative stress as a part of the host-parasite interaction, could potentially exacerbate the disease or lead to off-target effects that need to be determined.

RESOURCE AVAILABILITY

Lead contact

Further information and requests for resources and reagents should be directed to and will be fulfilled by the lead contact, Lise Lefèvre (lise.lefevre@univ-tlse3.fr).

Materials availability

This study did not generate new unique reagents.

Data and code availability

- Data reported in this paper will be shared by the lead contact upon request.
- This paper does not report original code.
- Any additional information required to reanalyze the data reported in this work paper is available from the lead contact upon request.

ACKNOWLEDGMENTS

We thank Philippe Batigne and Bénédicte Bertrand (Université Paul Sabatier) for excellent technical support and Jean Loup Lemesre (UMR INTERTRYP, Montpellier) for providing the cloned line of *L.i.* (MHOM/MA/67/ITMAP-263) expressing luciferase activity.

AUTHOR CONTRIBUTIONS

C.B., E.M., L.L., and A.C. designed the study and analyzed the data. C.B., M.L., K.C., M.S., M.T., R.P., H.A., K.S., G.J., M.R., M.P., I.R.L., and L.L. performed and analyzed the experiments. C.B., G.L.-V., E.M., L.L., and A.C. wrote the manuscript.

DECLARATION OF INTERESTS

The authors declare no competing interests.

STAR★METHODS

Detailed methods are provided in the online version of this paper and include the following:

- KEY RESOURCES TABLE

SUPPLEMENTAL INFORMATION

Supplemental information can be found online at https://doi.org/10.1016/j.celrep.2024.114720.

Received: October 20, 2023
Revised: April 4, 2024
Accepted: August 20, 2024
Published: September 7, 2024

REFERENCES

1. Mann, S., Frasca, K., Scherrer, S., Henao-Martínez, A.F., Newman, S., Ramanan, P., and Suarez, J.A. (2021). A Review of Leishmaniasis: Current Knowledge and Future Directions. Curr. Trop. Med. Rep. *8*, 121–132.
2. Murray, H.W., Berman, J.D., Davies, C.R., and Saravia, N.G. (2005). Advances in leishmaniasis. Lancet *366*, 1561–1577.
3. Kaye, P., and Scott, P. (2011). Leishmaniasis: complexity at the host-pathogen interface. Nat. Rev. Microbiol. *9*, 604–615.
4. Lefèvre, L., Lugo-Villarino, G., Meunier, E., Valentin, A., Olagnier, D., Authier, H., Duval, C., Dardenne, C., Bernad, J., Lemesre, J.L., et al. (2013). The C-type lectin receptors dectin-1, MR, and SIGNR3 contribute both positively and negatively to the macrophage response to Leishmania infantum. Immunity *38*, 1038–1049.
5. Vomund, S., Schäfer, A., Parnham, M.J., Brüne, B., and von Knethen, A. (2017). Nrf2, the Master Regulator of Anti-Oxidative Responses. Int. J. Mol. Sci. *18*, 2772.
6. Ngo, V., and Duennwald, M.L. (2022). Nrf2 and Oxidative Stress: A General Overview of Mechanisms and Implications in Human Disease. Antioxidants *11*, 2345.
7. Thimmulappa, R.K., Lee, H., Rangasamy, T., Reddy, S.P., Yamamoto, M., Kensler, T.W., and Biswal, S. (2006). Nrf2 is a critical regulator of the innate immune response and survival during experimental sepsis. J. Clin. Invest. *116*, 984–995.
8. Lin, W., Wu, R.T., Wu, T., Khor, T.O., Wang, H., and Kong, A.N. (2008). Sulforaphane suppressed LPS-induced inflammation in mouse peritoneal macrophages through Nrf2 dependent pathway. Biochem. Pharmacol. *76*, 967–973.
9. Bichiou, H., Rabhi, S., Ben Hamda, C., Bouabid, C., Belghith, M., Piquemal, D., Trentin, B., Rabhi, I., and Guizani-Tabbane, L. (2021). Leishmania Parasites Differently Regulate Antioxidant Genes in Macrophages Derived From Resistant and Susceptible Mice. Front. Cell. Infect. Microbiol. *11*, 748738.
10. Pang, Z., Xu, Y., and Zhu, Q. (2021). Early Growth Response 1 Suppresses Macrophage Phagocytosis by Inhibiting NRF2 Activation Through Upregulation of Autophagy During Pseudomonas aeruginosa Infection. Front. Cell. Infect. Microbiol. *11*, 773665.
11. Herengt, A., Thyrsted, J., and Holm, C.K. (2021). NRF2 in Viral Infection. Antioxidants *10*, 1491.
12. Vivarini, A.d.C., and Lopes, U.G. (2019). The Potential Role of Nrf2 Signaling in Leishmania Infection Outcomes. Front. Cell. Infect. Microbiol. *9*, 453.
13. Reverte, M., Eren, R.O., Jha, B., Desponds, C., Snäkä, T., Prevel, F., Isorce, N., Lye, L.F., Owens, K.L., Gazos Lopes, U., et al. (2021). The antioxidant response favors Leishmania parasites survival, limits inflammation and reprograms the host cell metabolism. PLoS Pathog. *17*, e1009422.
14. Saha, S., Roy, S., Dutta, A., Jana, K., and Ukil, A. (2021). Leishmania donovani Targets Host Transcription Factor NRF2 To Activate Antioxidant Enzyme HO-1 and Transcriptional Repressor ATF3 for Establishing Infection. Infect. Immun. *89*, e0076420.
15. Saha, S., Basu, M., Guin, S., Gupta, P., Mitterstiller, A.M., Weiss, G., Jana, K., and Ukil, A. (2019). Leishmania donovani Exploits Macrophage Heme Oxygenase-1 To Neutralize Oxidative Burst and TLR Signaling-Dependent Host Defense. J. Immunol. *202*, 827–840.
16. Song, X., and Long, D. (2020). Nrf2 and Ferroptosis: A New Research Direction for Neurodegenerative Diseases. Front. Neurosci. *14*, 267.
17. Dodson, M., de la Vega, M.R., Cholanians, A.B., Schmidlin, C.J., Chapman, E., and Zhang, D.D. (2019). Modulating NRF2 in Disease: Timing Is Everything. Annu. Rev. Pharmacol. Toxicol. *59*, 555–575.
18. Anandhan, A., Dodson, M., Schmidlin, C.J., Liu, P., and Zhang, D.D. (2020). Breakdown of an Ironclad Defense System: The Critical Role of NRF2 in Mediating Ferroptosis. Cell Chem. Biol. *27*, 436–447.
19. Bogacz, M., and Krauth-Siegel, R.L. (2018). Tryparedoxin peroxidase-deficiency commits trypanosomes to ferroptosis-type cell death. Elife *7*, e37503.
20. Bagayoko, S., and Meunier, E. (2022). Emerging roles of ferroptosis in infectious diseases. FEBS J. *289*, 7869–7890.
21. Saha, A., Biswas, A., Srivastav, S., Mukherjee, M., Das, P.K., and Ukil, A. (2014). Prostaglandin E2 negatively regulates the production of inflammatory cytokines/chemokines and IL-17 in visceral leishmaniasis. J. Immunol. *193*, 2330–2339.
22. Gjyshi, O., Flaherty, S., Veettil, M.V., Johnson, K.E., Chandran, B., and Bottero, V. (2015). Kaposi's Sarcoma-Associated Herpesvirus Induces Nrf2 Activation in Latently Infected Endothelial Cells through SQSTM1 Phosphorylation and Interaction with Polyubiquitinated Keap1. J. Virol. *89*, 2268–2286.
23. Wang, L., Zhang, X., Xiong, X., Zhu, H., Chen, R., Zhang, S., Chen, G., and Jian, Z. (2022). Nrf2 Regulates Oxidative Stress and Its Role in Cerebral Ischemic Stroke. Antioxidants *11*, 2377.
24. Zhou, B., Liu, J., Kang, R., Klionsky, D.J., Kroemer, G., and Tang, D. (2020). Ferroptosis is a type of autophagy-dependent cell death. Semin. Cancer Biol. *66*, 89–100.
25. Huang, W., Li, H., Kiselar, J., Fink, S.P., Regmi, S., Day, A., Yuan, Y., Chance, M., Ready, J.M., Markowitz, S.D., and Taylor, D.J. (2023). Small molecule inhibitors of 15-PGDH exploit a physiologic induced-fit closing system. Nat. Commun. *14*, 784.
26. Kobayashi, E.H., Suzuki, T., Funayama, R., Nagashima, T., Hayashi, M., Sekine, H., Tanaka, N., Moriguchi, T., Motohashi, H., Nakayama, K., and Yamamoto, M. (2016). Nrf2 suppresses macrophage inflammatory response by blocking proinflammatory cytokine transcription. Nat. Commun. *7*, 11624.
27. Sundar, S., and Chakravarty, J. (2010). Liposomal Amphotericin B and Leishmaniasis: Dose and Response. J. Global Infect. Dis. *2*, 159–166.
28. Basmaciyan, L., and Casanova, M. (2019). Cell death in Leishmania. Parasite *26*, 71.
29. Wang, T., Jing, B., Xu, D., Liao, Y., Song, H., Sun, B., Guo, W., Xu, J., Li, K., Hu, M., et al. (2020). PTGES/PGE2 signaling links immunosuppression and

lung metastasis in Gprc5a-knockout mouse model. Oncogene *39*, 3179–3194.

30. Zhang, Y., Desai, A., Yang, S.Y., Bae, K.B., Antczak, M.I., Fink, S.P., Tiwari, S., Willis, J.E., Williams, N.S., Dawson, D.M., et al. (2015). TISSUE REGENERATION. Inhibition of the prostaglandin-degrading enzyme 15-PGDH potentiates tissue regeneration. Science *348*, aaa2340.
31. Singh, A., Venkannagari, S., Oh, K.H., Zhang, Y.Q., Rohde, J.M., Liu, L., Nimmagadda, S., Sudini, K., Brimacombe, K.R., Gajghate, S., et al. (2016). Small Molecule Inhibitor of NRF2 Selectively Intervenes Therapeutic Resistance in KEAP1-Deficient NSCLC Tumors. ACS Chem. Biol. *11*, 3214–3225.
32. Bagayoko, S., Leon-Icaza, S.A., Pinilla, M., Hessel, A., Santoni, K., Péricat, D., Bordignon, P.J., Moreau, F., Eren, E., Boyancé, A., et al. (2021). Host phospholipid peroxidation fuels ExoU-dependent cell necrosis and supports Pseudomonas aeruginosa-driven pathology. PLoS Pathog. *17*, e1009927.
33. Itoh, K., Chiba, T., Takahashi, S., Ishii, T., Igarashi, K., Katoh, Y., Oyake, T., Hayashi, N., Satoh, K., Hatayama, I., et al. (1997). An Nrf2/small Maf heterodimer mediates the induction of phase II detoxifying enzyme genes through antioxidant response elements. Biochem. Biophys. Res. Commun. *236*, 313–322.
34. Olagnier, D., Lavergne, R.A., Meunier, E., Lefèvre, L., Dardenne, C., Aubouy, A., Benoit-Vical, F., Ryffel, B., Coste, A., Berry, A., and Pipy, B. (2011). Nrf2, a PPARγ alternative pathway to promote CD36 expression on inflammatory macrophages: implication for malaria. PLoS Pathog. *7*, e1002254.
35. Hirano, K., Chen, W.S., Chueng, A.L.W., Dunne, A.A., Seredenina, T., Filippova, A., Ramachandran, S., Bridges, A., Chaudry, L., Pettman, G., et al. (2015). Discovery of GSK2795039, a Novel Small Molecule NADPH Oxidase 2 Inhibitor. Antioxidants Redox Signal. *23*, 358–374.

STAR★METHODS

KEY RESOURCES TABLE

REAGENT or RESOURCE	SOURCE	IDENTIFIER
Antibodies		
Mouse anti-Cox2	BD Transduction Laboratories	Cat# 610204 RRID:AB_397603
Rabbit anti-Pges	Invitrogen	Cat# 702796 RRID:AB_2734827
Rabbit anti-Ptger2	Invitrogen	Cat# MA5-35750 RRID:AB_2849650
Mouse anti-βactin	Santa Cruz Biotechnology	Cat# sc-69879 RRID:AB_1119529
Rabbit anti-Nrf2	Invitrogen	Cat# MA5-42371 RRID:AB_2911512
Goat anti-Rabbit IgG Alexa Fluor™ 488	Invitrogen	Cat# A-11008 RRID:AB_143165)
Mouse anti-Heme Oxygenase	Santa Cruz Biotechnology	Cat# sc-136960 RRID:AB _2011613
Mouse anti -NQO1	Santa Cruz Biotechnology	Cat# sc-32793 RRID:AB_628036
Rabbit anti-Nrf2	Santa Cruz Biotechnology	Cat# sc-13032 RRID:AB_2263168
Biological samples		
Blood Peripheral Blood Mononuclear Cells (PBMCs)	French Blood Institute	N/A
Chemicals, peptides, and recombinant proteins		
AH6809 (EP2 antagonist)	Sigma-Aldrich	Cat# A1221-5MG
Trolox	Sigma-Aldrich	Cat# 238813-1G
GSK2795039 (NOX2 inhibitor)	Sigma-Aldrich	Cat# SML2770-1MG
SW033291 (15-PGDH inhibitor)	Sigma-Aldrich	Cat# SML1485-5MG
ML385 (Nrf2 inhibitor)	Sigma-Aldrich	Cat# SML1833-25MG
CAY10526 (pges inhibitor)	Sigma-Aldrich	Cat# SML2530-5MG
NS-398 (Cox-2 inhibitor)	Sigma-Aldrich	Cat# N194-5MG
Ferrostatin-1	Sigma-Aldrich	Cat# SML0583-25MG
PGE2	Cayman Chemical	Cat# CAYM14010-10
Liposomal amphotericin B (Ambisome)	This paper	N/A
Hydrogen peroxide	Thermo Scientific	Cat# 202465000
RIPA Buffer	Sigma-Aldrich	Cat# R0278
Recombinant Human M-CSF	PeproTech	Cat# 300-25
Ficoll 1.077 ± 0.001 g/mL	GE Healthcare	Cat# 17-1441-02
DMEM	Sigma-Aldrich	Cat# D0822-500ML
Fetal Bovin Serum	Invitrogen	Cat# 10082147
RPMI 1640	Fisher Scientific	Cat# 12027599
Penicillin-streptomycin	Fisher Scientific	Cat# 11548876
5-amino-2,3-dihydro-1,4-phthalazinedione	Sigma-Aldrich	Cat# A8511
PD0325901	Selleckchem	Cat# S1036
Skepinone-L	Clinisciences	Cat# HY-15300
H89	Sigma-Aldrich	Cat# B1427-5MG
Staurosporin	Sigma-Aldrich	Cat# 19-123

(*Continued on next page*)

Continued

REAGENT or RESOURCE	SOURCE	IDENTIFIER
Sulfanilamide	Fisher Scientific	Cat# 11479893
naphthylethylenediamine dihydrochloride	Sigma-Aldrich	Cat# 222488-5G
G418 sulfate (geneticin)	Fisher Scientific	Cat# 10131027
luciferase substrate	Promega	Cat# E2520
Critical commercial assays		
BODIPY™ 581/591 C11 (Lipid Peroxidation Sensor)	Invitrogen	Cat# D3861
AlamarBlue™ Cell Viability Reagent	Invitrogen	Cat# DAL1025
Nuclear Extract Kit	Active Motif	Cat# 40010
TransAM® Nrf2	Active Motif	Cat# 50296
Verso cDNA kit	Thermo Fisher Scientific	Cat# AB1453B
LightCycler SYBR Green I Master	Roche Diagnostics	Cat# 4887352001
High Pure PCR Template preparation kit	Roche Diagnostics	Cat# 11796828001
PGEM EIA Kit	Cayman Chemical	Cat# 514531
PGE2 EIA Kit	Cayman Chemical	Cat# 514010
8-Isoprostane EIA Kit	Cayman Chemical	Cat# 516351
Human IL-1beta Uncoated ELISA Kit	Thermo Fisher Scientific	Cat# 88-7261-88 RRID:AB_2575054
Human IL-10 Uncoated ELISA Kit	Thermo Fisher Scientific	Cat# 88-7106-22 RRID:AB_2575001
Human/Mouse TGF-beta uncoated ELISA	Thermo Fisher Scientific	Cat# 88-8350-88 RRID:AB_2575211
Human IL-6 Uncoated ELISA Kit	Thermo Fisher Scientific	Cat# 88-7066-88 RRID:AB_2574995
Human TNF alpha Uncoated ELISA Kit	Thermo Fisher Scientific	Cat# 88-7346-88 RRID:AB_2575097
Human IL-12p70 Uncoated ELISA Kit	Thermo Fisher Scientific	Cat# 88-7126-88 RRID:AB_2575023
Mouse IL-1beta Uncoated ELISA Kit	Thermo Fisher Scientific	Cat# 88-7013-22 RRID:AB_2574942
Mouse TNF alpha Uncoated ELISA Kit	Thermo Fisher Scientific	Cat# 88-7324-22 RRID:AB_2575076
Mouse IL-10 Uncoated ELISA Kit	Thermo Fisher Scientific	Cat# 88-7105-88 RRID:AB_2574997
Mouse IL-6 Uncoated ELISA Kit	Thermo Fisher Scientific	Cat# 88-7064-22 RRID:AB_2574986
Mouse IL-12 Uncoated ELISA Kit	Thermo Fisher Scientific	Cat# 88-7121-88 RRID:AB_2575018
Clarity™ Western ECL Substrate	Biorad	Cat# 1705060
Total RNA Miniprep Super Kit	BioBasic	Cat# BS784
Human pan monocyte isolation kit	Miltenyi Biotec	Cat# 130-100-629
Experimental models: Organisms/strains		
C57BL/6J	The Jackson laboratory	Cat # JAX: 000664, RRID: IMSR_JAX: 000664
Nfe2l2$^{+/+}$ and Nfe2l2$^{-/-}$ mice	Itoh et al.[29]	N/A
129S2/SvPasOrlRj	Janvier Labs	Cat # SC-129SV-M
Leishmania infantum-luc MHOM/MA/67/ ITMAP-263	Laboratory of Dr. Jean-Loup Lemesre	N/A
Oligonucleotides		
qPCR primers, see Table S1: Primer sequences	This paper	N/A
Software and algorithms		
GraphdPad Prism 8.0 for Windows	GraphPad Software, La Jolla California USA	https://www.graphpad.com/scientific-software/prism/

EXPERIMENTAL MODEL AND STUDY PARTICIPANT DETAILS

Mice

All mouse experiments were performed according to protocols approved by the institutional ethics committee CEEA - 001 ‘‘Comité d’éthique en expérimentation animale de la Fédération de Recherche en Biologie de Toulouse (FRBT)’’ (ethics committee number 122, US006/CREFFRE) with permit number 6555–2016082912056664 and 2019112715257559 in accordance with European legal

and institutional guidelines (2010/63/UE) for the care and use of laboratory animals. All mice were bred in the same facility, and age-matched wild type mice were first co-housed with genetically modified mice just after weaning at 3 weeks old for at least 4 weeks before use. At the start of the experiments, animals weighed (mean ± SD) 24 ± 0.36 g and were 6-week-old male. Animals were housed in 425 × 266 × 185 mm cages (Tecniplast, 1291H Type III H, France) and given access to maintenance food (Global Diet, Harlan, France) and water *ad libitum*. The photoperiod was adjusted to 12 h light and 12 h dark and ambient temperature was maintained at 20°C +/− 1°C. Environmental enrichment included bedding and one hut. The experimenters were blinded to the mice genotype for monitoring animals. The *Nfe2l2*+/+ and *Nfe2l2*$^{-/-}$ *(C57BL/6)* mice have been provided by Dr. Itoh and bred in our facility.[33,34] The *C57BL/6J* mice and *129/Sv* mice were purchased from Janvier Labs.

Leishmania cell culture

The cloned line of *Leishmania infantum* (MHOM/MA/67/ITMAP-263) and the axenic amastigotes expressing luciferase activity (*L.i.*-luc) have been provided by J.L Lemesre.[4] For animal and macrophage infection and *in vitro* experiments, the parasites were transformed in promastigotes by changes in culture conditions (25°C and RPMI 10% fetal calf serum Cat# 10082147 with G418 at 50 μg/mL, Cat# 10131027). Medium was changed every 3 days.

METHOD DETAILS

Visceral leishmaniasis model

For the *in vivo* experiments, a visceral infection was established by inoculating i.p. 50× 10^6 stationary phase promastigotes into 6-week-old male mice.[4] At 14 days after infection, the liver, spleen and peritoneal macrophages were removed aseptically. Mice were treated with an ROS chelator (Trolox[23] 40 mg/kg, Sigma-Aldrich) every 2 days; a cocktail of PGEs inhibitor (CAY10526[29] 5 mg/kg, Sigma-Aldrich) and prostanoid receptor antagonist 2 (AH6808[21] 5 mg/kg, Sigma-Aldrich) every 2 days; a 15-PGDH inhibitor (SW033291[30] at 10 mg/kg, Sigma-Aldrich) every 2 days; an Nrf2 inhibitor (ML385[31] at 10 mg/kg, Sigma-Aldrich) every two days; or liposomal amphotericin B (Ambisome 3 mg/kg, Sigma-Aldrich) at day 0, 1, 2, 3, 4 and 10. Mice were treated with Fe-1[32] (10 mg/kg, Sigma-Aldrich) each day.

For adoptive transfers, peritoneal macrophages from three Nfe2l2$^{-/-}$ donor mice were collected and transferred (*i.p.*) into the corresponding Nfe2l2$^{+/+}$ recipient mouse model (n = 6) 10 h before *L.i.* infection. Liver and spleen were isolated and peritoneal macrophages were harvested 14 days after infection.

Mouse peritoneal macrophages isolation

Resident peritoneal cells were harvested by washing the peritoneal cavity with sterile 0.9% NaCl. Collected cells were centrifuged and the cell pellet was suspended in DMEM with 5% FBS (Cat# D0822-500ML). Cells were allowed to adhere for 2 h at 37°C, 5% CO2. Non-adherent cells were then removed by washing with PBS.

Purification and generation of monocyte-derived macrophages

Monocytes were isolated from blood Peripheral Blood Mononuclear Cells (PBMCs) from healthy donors obtained from the EFS Toulouse Purpan (France). Briefly, PBMCs were isolated by centrifugation using standard Ficoll-Paque density (Cat# 17-1441-02), according to the manufacturer's instructions. The cells were re-suspended in RPMI-1640 supplemented with 10% of fetal calf serum (FCS, Cat# 10082147), 1% penicillin (100 IU/mL) and streptomycin (100 μg/mL) (Cat# 11548876). Monocytes were separated by negative selection using Pan monocyte isolation kit (Cat# 130-100-629). Cells were cultured in RPMI-1640 (Cat# 12027599) supplemented with 10% FCS, 100 IU/mL penicillin, 100 μg/mL streptomycin, 10 ng/mL M-CSF (Cat# 300-25) for 5 days at 37°C under a 5% CO_2 humidified atmosphere.

Reverse transcription and Real-time PCR

Adherent murine peritoneal macrophages were pre-treated 24 h before *L.i.* challenge (parasite-to-macrophage ratio 5:1) with PD0325901 MEK/ERK inhibitor (Cat# S1036), Skepinone-L (P38 MAPK inhibitor) (Cat# HY-15300), H89 (PKA inhibitor) (Cat# B1427-5MG), Staurosporin (PKC inhibitor) (Cat# 19–123).

The mRNA of interest was isolated using the biobasic Kit (Cat# BS784) using the manufacturer's protocol. Synthesis of cDNA was performed according to the manufacturer's recommendations (Cat# AB1453B). RT–qPCR was performed on a LightCycler 480 system using LightCycler SYBR Green I Master (Cat# 4887352001). The primers were designed with the software Primer 3. Glyceraldehyde-3-phosphate dehydrogenase (Gapdh) mRNA was used as the invariant control. Serially diluted samples of pooled cDNA were used as external standards in each run for the quantification. Primer sequences are listed in Table S1.

Quantification of L. *infantum* in liver and spleen

L. infantum DNA was purified using High Pure PCR Template preparation kit (Cat# 11796828001). The LightCycler PCR and detection system () was used for amplification and quantification. For amplicon detection, LightCycler SYBR Green I Master (Cat# 4887352001) was used on a LightCycler 480 system.

Primers (5′GTGGGGGAGGGGCGTTCT3′, 5′ATTTTACACCAACCCCCAGTT3′) bind to conserved regions of kDNA minicircle.

Proliferation and phagocytosis assays

Adherent murine peritoneal macrophages were pre-treated 24 h before *L.i.* challenge (parasite-to-macrophage ratio 5:1) with GSK2795039[35] (10 μM Cat# SML2770-1MG), AH6808[21] (Cat# A1221-5MG, 10 μM), SW03329 (10 μM, Cat# SML1485-5MG), NS398 (10 μM, Cat# N194-5M), CAY10526 (10 μM), PGE2 (1 μM Cat# CAYM14010-10) or ML385 (10 μM). To evaluate, phagocytosis and proliferation of *L.i.*, the macrophages were challenged with *L.i.*-luc for 30 min at 37°C (phagocytosis) and for 24 h at 37°C (proliferation). Macrophage were then lysed and the luciferase substrate (Cat# E2520) was added. The luciferase activity was measured with a luminometer (Envison, PerkinElmer).

ROS and NO production, ELISA cytokine Titration, and EIA lipid quantification

The ROS production by macrophages was measured by chemiluminescence monitoring in the presence of 5-amino-2,3-dihydro-1,4-phthalazinedione (luminol, Cat# A8511)) using a thermostatically (37°C) controlled Envision (PerkinElmer) continuously for 1 h after *L.i.* challenge quantification was performed using the area under the curve expressed in counts x seconds. For nitrite release, Griess reagent was used to quantify the concentration of nitrite, which is a stable product of NO. Briefly, culture medium of macrophages was incubated with equal volumes of a solution containing 1% sulfanilamide (Cat# 11479893) and 0.1% naphthylethylenediamine dihydrochloride (Cat# 222488-5G) in 2.5% phosphoric acid. After 30 min at room temperature, the absorbance was read at 550 nm by comparison with standard solutions of sodium nitrite prepared in the same culture media. The cytokine releases were evaluated by ELISA in cell supernatants or in peritoneal fluids (IL-1β, IL-12, IL-6, TNFα, TGFβ, IL-10 BD Biosciences, R&D Systems) according to the manufacturer's instructions. The 8-isoprostane (Cat# 514531), PGE2 (Cat# 514010) and PGEM (Cat# 514531) were quantified using EIA kits, as recommended by the manufacturer's protocols.

Immunoblotting

Total protein lysates were extracted according to standard procedures. After protein transfer, the membranes were incubated with either anti-Cox2 antibody (Cat# 610204, RRID: AB_397603), anti-Pges (Cat# 702796, RRID: AB_2734827), anti-Ptger2 (Cat# MA5-35750, RRID: AB_2849650), anti-HMOX1 (Cat# sc-136960 RRID: AB _2011613), anti-NQO1 (Cat# sc-32793 RRID: AB_628036), anti-Nrf2 (Cat# sc-13032 RRID: AB_2263168) or anti-β-actin (Cat# sc-69879, RRID: AB_1119529). Immunoblottings were revealed using a chemiluminescent substrate ECL substrate (Cat# 1705060) and the images were acquired on a ChemiDoc Imaging System (Bio-rad). Protein amounts were quantified using Fiji (ImageJ) software and normalized to the loading control β-actin. In each western blot, the molecular weight (kDa) of the most adjacent molecular weight marker is shown.

Fluorescence imaging confocal microscopy

Murine or human macrophages were fixed with PBS containing 4% paraformaldehyde. After permeabilization and blocking, cells were incubated at 4°C with anti-Nrf2 antibody (Cat# MA5-42371, RRID: AB_2911512) and then an anti-rabbit Alexa 488 antibody was used (Cat# A-11008 (also A11008), RRID: AB_143165). Nuclei were stained with DAPI. All microscopy imagery was performed with an Operetta high content quantitative confocal imaging (PerkinElmer). For each condition, 60 000 cells were analyzed. The staining was representative of three independent experiments. At least sixty-fields/well with a minimum of 3Z planes were analyzed with integrated Columbus image analysis software. Image analysis was performed and the cells-total number, mean/well cell–Alexa Fluor intensity, was computed. Nuclear translocation of Nrf2 was obtained by Alexa 488 fluorescence intensity in DAPI fluorescence intensity. Briefly, images were acquired using Operetta High Content Analysis system (Revvity) with 20x Air/0.45 NA. DAPI and Nrf2 were excited with the 360-400nm and 460-490nm excitation filters respectively. Nuclei were segmented with 'Find nuclei' building block of the Harmony Analysis Software (Revvity). Intensity of Nrf2 labeling in the nuclei: ROI were calculated using the 'Calculate Intensity Properties' building block and normalized by intensity values of the background noise, for each well.

Nuclear protein extraction and DNA-binding activity

Peritoneal macrophages from wild-type mice were previously treated for 24 h with the NOX2 inhibitor GSK2795039 at 10 μM (Cat# SML2770-1MG), or the PGEs inhibitor CAY10526 at 10 μM (Cat# SML2530-5MG) and the EP2 receptor inhibitor AH6808 (10 μM, Cat# A1221-5MG). After washing with PBS−/−, macrophages were infected with *L.i.* (1/5 ratio) for 4 h or 48 h. Nuclear proteins were isolated according to the manufacturer instruction (Cat# 40010). Nrf2 TransAM ELISA-kit (Cat# 50296) was used to evaluate Nrf2 DNA-binding activity. The absorbance was measured at 450 nm on a microplate reader (Envision PerkinElmer).

Leishmania lipid peroxidation

To measure lipid peroxidation of *Leishmania infantum* parasites in macrophages, *L.i.* was incubated with C11-BODIPY (581/591) (Cat# D3861) at 2 μM, in Opti-MEM medium for 2 h at 25°C. After washes with PBS, *L.i.* was resuspended in RPMI 10% FBS in the presence (or absence) of H_20_2 at 100 μM (Cat# 202465000), or ferrostatin-1 (Cat# SML0583-25MG) at 20 μm for 4 h at 37°C. Lipid peroxidation was assessed by measuring the fluorescence of C11-BODIPY at 488 nm using (BD FORTESSA or PerkinElmer Envision plate reader).

L.i. (pre-incubated with C11-BODIPY) was also challenged with mouse peritoneal macrophages (Nrf2 $^{+/+}$) or (Nrf2 $^{-/-}$) pre-treated (or not) with ML385 (10 μM, Cat# SML1833-25MG), or with h-MDM pre-treated with ML385 (10 μM, Cat# SML1833-25MG). After 1h30 of infection, cells were washed with PBS to remove extracellular *L.i.* and incubated for 4 h. Lipid peroxidation was assessed

by measuring the change in fluorescence of C11-BODIPY at 488 nm using direct fluorescence reading with the plate reader (Envision PerkinElmer).

Cell viability

Cell viability of *L.i.*-infected macrophages or *L.i.* promastigotes alone was assessed using the AlamarBlue proliferation assay (Cat# DAL1025), according to the manufacturer's instructions. AlamarBlue reagent was incubated for 4 h. The fluorescence intensity was measured with a fluorescence plate reader (Varioskan Thermo fisher scientific) with an excitation of 560 nm and an emission of 590 nm. The results were expressed as the percentage of viable cells compared to uninfected macrophages.

QUANTIFICATION AND STATISTICAL ANALYSIS

The statistical analyses in this study were performed using GraphPad Prism software (GraphPad v9.5). Data are shown as mean ± standard error of the mean (SEM) and are representative of at least three biological replicates with 3 technical replicates unless otherwise stated. Statistical significance analysis was determined by using unpaired Student's t-test or one-way ANOVA analysis. The statistical parameters for each experiment are reported in the respective figure legend. Significance was assumed with $p < 0.05$ and is indicated in the figures.